Ingeniería Solidaria

Phyllot: mobile robot for piping inspection: control modeling and simulation integrating solidworks®, simscape multibody®, and simulink®

Phyllot: robot móvil para inspección de tuberías: modelado y simulación del control integrando solidworks®, simscape multibody® y simulink®

Phyllot: Robô móvel para inspeção de tubulações: modelagem e simulação de controle integrando SolidWorks®, Simscape Multibody® e Simulink®

Juan Carlos Casas-Bustos[1]
Juan Jairo Vaca-González[2]
Esteban A. Rodríguez-Meléndez[3]

Received: June 24th, 2025
Accepted: November 15th, 2025
Available: January 13th, 2026

How to cite this article:
J.C. Casas-Bustos, J.J. Vaca-González, and E.A. Rodríguez-Meléndez, "PHYLLOT: Mobile Robot for Piping Inspection: Control Modeling and Simulation Integrating SolidWorks®, Simscape Multibody®, and Simulink®," *Revista Ingeniería Solidaria,* vol. 22, no. 1, 2026.
doi: https://doi.org/10.16925/2357-6014.2026.01.10

Research article. https://doi.org/10.16925/2357-6014.2026.01.10

[1] Researcher, SciBas Research Group and EUREKA Research Group, Research Office, Faculty of Technology (ODI), Universidad Distrital Francisco José de Caldas, Bogotá D.C., Colombia.
E-mail: jccasasb@udistrital.edu.co
ORCID: https://orcid.org/0009-0008-8924-1201
CvLAC: https://scienti.minciencias.gov.co/cvlac/visualizador/generarCurriculoCv.do?cod_rh=0002439359

[2] Professor, Academic Directorate, Universidad Nacional de Colombia, La Paz Campus; Biodiversity for Society Research; Biomimetics Laboratory, Biotechnology Institute; Numerical Methods and Modeling Research Groups, Universidad Nacional de Colombia, Colombia.
E-mail: [agregar correo electrónico]
ORCID: https://orcid.org/0000-0003-3829-2558
CvLAC: https://scienti.minciencias.gov.co/cvlac/visualizador/generarCurriculoCv.do?cod_rh=0001399168

[3] Researcher, Nanostructures and Applied Physics Research Group, Academic Directorate, Universidad Nacional de Colombia, La Paz Campus, Colombia.
E-mail: [agregar correo electrónico]
ORCID: https://orcid.org/0000-0002-2612-3960
CvLAC: https://scienti.minciencias.gov.co/cvlac/visualizador/generarCurriculoCv.do?cod_rh=0001708541

Abstract

Introduction: This paper presents the final results of the research project conducted at Universidad Distrital Francisco José de Caldas in 2025 on a solution for the in situ internal inspection of PIG-type industrial pipelines through the design, automation, and virtual control of a parameterized unmanned robotic vehicle, **PhylloT**, inspired by the Colombian poison dart frog (*Phyllobates terribilis*).

Problem: Inspection devices or sensing probes inserted into pipelines often operate under harsh conditions as open-loop systems with insufficient control mechanisms and incomplete feedback.

Objective: To develop a virtual robot design based on functional conditions inspired by biological behaviors adapted to the branching of circular cross-section pipelines.

Methods: The simulation model was developed, integrated, and programmed in SolidWorks®; the components and assembly were exported to Simscape Multibody® for implementation in Simulink® within MATLAB® and validated using SolidWorks® Motion.

Results: Virtual simulations maintained the parameterization of the integrated system within the SolidWorks® Motion® platform. The final control variable, represented by the position sampled through animation frames, generated linear and angular velocities, linear and angular accelerations, and linear and angular displacements.

Conclusion: Virtual design, control, and automation systems provide effective solutions by directly validating the most relevant variables involved in PIG-type pipeline inspection.

Originality: This approach integrates CAD design technologies with mathematical modeling and simulation tools through open-code implementation and the validation of individual motion parameters that influence the robot's locomotion.

Limitations: The proposed parameterization is limited to basic spatial geometries. In addition, personnel must be trained in the use of robust computing platforms and possess prior knowledge of design and control software.

Keywords: modeling, simulation, automatic control, mobile robotics, pipeline inspection, SolidWorks®, Simscape Multibody®, Simulink®, MATLAB®, SolidWorks Motion®.

Resumen

Introducción: Este artículo presenta los resultados finales de la investigación desarrollada en la Universidad Distrital Francisco José de Caldas durante el año 2025, orientada a resolver el problema de la inspección interna *in situ* de tuberías industriales tipo PIG mediante el diseño, la automatización y el control virtual de un robot no tripulado parametrizado, denominado **PhylloT**, inspirado en la rana dardo venenosa colombiana (*Phyllobates terribilis*).

Problema: Los dispositivos de inspección o sondas de reconocimiento insertados en tuberías suelen operar en condiciones adversas como sistemas de lazo abierto, con mecanismos de control insuficientes y retroalimentación incompleta.

Objetivo: Desarrollar un diseño virtual de un robot basado en condiciones funcionales inspiradas en comportamientos biológicos, adaptados a la ramificación de tuberías de sección transversal circular.

Métodos: El modelo de simulación fue desarrollado, integrado y programado en SolidWorks®; posteriormente, los componentes y el ensamblaje se exportaron a Simscape Multibody® para su implementación en Simulink® de MATLAB® y su validación mediante SolidWorks® Motion.

Resultados: Las simulaciones realizadas en un entorno virtual mantuvieron la parametrización del sistema integrada en la plataforma SolidWorks® Motion®. La variable final de control, representada por la posición muestreada mediante fotogramas de la simulación, permitió generar velocidades, aceleraciones y desplazamientos tanto lineales como angulares.

Conclusión: Los sistemas virtuales de diseño, control y automatización proporcionan soluciones eficientes al permitir la validación directa de las variables más relevantes involucradas en la inspección de tuberías tipo PIG.

Originalidad: Este enfoque integra tecnologías de diseño asistido por computador (CAD) con herramientas de modelado matemático y simulación, mediante codificación abierta y la validación de parámetros individuales de movimiento que influyen en la locomoción del robot.

Limitaciones: La parametrización propuesta se limita a geometrías espaciales básicas. Además, el personal debe estar capacitado en el uso de plataformas computacionales robustas y contar con conocimientos previos en programas de diseño y control.

Palabras clave: modelado, simulación, control automático, robótica móvil, inspección de tuberías, SolidWorks®, Simscape Multibody®, Simulink®, MATLAB®, SolidWorks Motion®.

Resumo

Introdução: Este artigo apresenta os resultados finais de uma pesquisa realizada na Universidade Distrital Francisco José de Caldas durante o ano de 2025, com o objetivo de solucionar o problema da inspeção interna in situ de tubulações industriais do tipo PIG por meio do projeto, automação e controle virtual de um robô não tripulado parametrizado, denominado PhylloT, inspirado no sapo-flecha-colombiano (Phyllobates terribilis).

Problema: Dispositivos ou sondas de inspeção inseridos em tubulações frequentemente operam em condições adversas como sistemas de malha aberta, com mecanismos de controle insuficientes e feedback incompleto.

Objetivo: Desenvolver um projeto de robô virtual baseado em condições funcionais inspiradas em comportamentos biológicos, adaptado à ramificação de tubulações com seção transversal circular.

Métodos: O modelo de simulação foi desenvolvido, integrado e programado no SolidWorks®; posteriormente, os componentes e a montagem foram exportados para o Simscape Multibody® para implementação no MATLAB® Simulink® e validação utilizando o SolidWorks® Motion. Resultados: As simulações realizadas em ambiente virtual mantiveram a parametrização do sistema integrada à plataforma SolidWorks® Motion®. A variável de controle final, representada pela posição amostrada usando quadros de simulação, permitiu a geração de velocidades lineares e angulares, acelerações e deslocamentos.

Conclusão: Sistemas virtuais de projeto, controle e automação fornecem soluções eficientes, permitindo a validação direta das variáveis mais relevantes envolvidas na inspeção de tubulações do tipo PIG.

Originalidade: Esta abordagem integra tecnologias de projeto auxiliado por computador (CAD) com ferramentas de modelagem e simulação matemática, utilizando código aberto e a validação de parâmetros de movimento individuais que influenciam a locomoção do robô.

Limitações: A parametrização proposta limita-se a geometrias espaciais básicas. Além disso, o pessoal deve ser treinado no uso de plataformas computacionais robustas e possuir conhecimento prévio de softwares de projeto e controle.

Palavras-chave: modelagem, simulação, controle automático, robótica móvel, inspeção de tubulações, SolidWorks®, Simscape Multibody®, Simulink®, MATLAB®, SolidWorks Motion®.

1. INTRODUCTION

In most industries, pipelines are essential components for transporting water, gas, petroleum derivatives, food, beverages, and many other products in liquid, solid, or gaseous form. Maintaining their integrity is crucial to ensuring operational safety, efficiency, and reliability while preventing failures and service interruptions. Consequently, pipeline inspection plays a fundamental role by enabling the detection and correction of engineering or installation defects, such as leaks, discontinuities, corrosion, or obstructions, before commissioning, thereby preventing costly operational failures.

Pipeline inspection can be performed using external propulsion equipment, commonly referred to as Pipeline Inspection Gauges (PIGs), or internal propulsion systems, known as Remotely Operated Vehicles (ROVs), which incorporate actuators that enable navigation inside pipelines while being remotely controlled by an external operator. In some applications, both approaches are combined using different inspection techniques and specialized tools. Traditionally, most studies have focused on visual inspection techniques for PIG systems; however, complementary methods such as Non-Destructive Testing (NDT), Eddy Current Testing, Magnetic Flux Leakage (MFL) testing, and Hydrostatic Testing are also widely employed.

Visual inspection is primarily conducted by an expert who may use systems such as Push Cameras, which are manually inserted and are suitable for short- and medium-length pipelines [1]; Robotic Cameras, equipped with wheels or alternative locomotion systems that autonomously navigate inside pipelines under remote supervision, making them suitable for long or difficult-to-access pipelines [1]; Pan-Tilt-Zoom (PTZ) cameras, which provide 360° views of the pipeline interior, enabling comprehensive condition assessment while being mounted on autonomous locomotion platforms [1]; Borescopes, consisting of rigid tubes equipped with optical lenses and illumination systems for direct visual inspection of inaccessible internal areas [2]; Videoscopes, which are similar to borescopes but include image and video recording capabilities for subsequent analysis [2]; and drones, which are employed for the external inspection of elevated or remote pipelines using high-resolution cameras and Global Positioning System (GPS) technology, although they are limited to external inspection tasks [2].

Alternative inspection methods to visual assessment include defect detection using machine learning techniques, ultrasonic inspection, magnetic flux leakage analysis, and pressure-based defect detection [3].

Regardless of the inspection technique employed, selecting an appropriate locomotion mechanism for traversing the pipeline network is essential to facilitate data acquisition and sample collection while ensuring the reliable transmission of inspection data to the diagnostic system [4].

From this perspective, the development of robotic solutions for dynamic environments containing a wide variety of industrial pipelines presents significant challenges, both in the design of locomotion mechanisms and in the implementation of robust control systems. Although horizontal pipelines are relatively straightforward to inspect, limited experience has been reported for inclined or vertical pipeline sections, particularly those containing joints or complex geometries.

Reference [4] presents the design of an inspection system based on a camera integrated into a non-holonomic mobile robot capable of acquiring real-time images and operational data. Similarly, [5] describes the implementation of a teleoperated four-wheeled non-holonomic robot equipped with a 360° vision camera that provides real-time images of the pipeline interior. Furthermore, [6] details the development of an autonomous robotic system capable of navigating long pipelines while acquiring accurate inspection images and operational data.

Nevertheless, although mobile robots are widely employed for pipeline inspection, they generally exhibit limited adaptability to the diverse geometric configurations and operating conditions encountered in industrial pipelines [7]. For example, in 2007, [8] presented the design of wheeled inspection robots suitable for circular pipelines with diameters ranging from 85 mm to 109 mm, based on a modular architecture incorporating pantograph mechanisms. Likewise, [9] proposed several geometries for a pipeline inspection robot; however, these configurations were limited to linear sections of vertical pipelines. Although these studies represent important advances, the proposed systems remain applicable only to relatively short pipeline sections that do not include sharp directional changes and maintain a constant diameter throughout the inspection path.

From a commercial perspective, numerous high-cost inspection solutions are currently available. Synthotech introduced the SynthoTrax robotic platform, a compact robotic vehicle designed for the inspection of metallic and polyethylene (PE) pipelines with diameters starting from 12 in (approximately 300 mm) [10]. This crawler-type vehicle can carry different types of inspection sensors; however, it lacks autonomous locomotion because it requires an insertion probe [11]. For the visual inspection of horizontal pipelines using Pan-Tilt-Zoom (PTZ) cameras, ABE Group [3] offers specialized tracking units. Similarly, the Versatrax 300, developed by Inuktun, incorporates a manually adjustable chassis capable of traversing horizontal pipeline sections with rectangular or circular cross-sections greater than 300 mm in diameter. The company also offers robotic platforms for vertical pipelines featuring pantograph adjustment mechanisms suitable for diameters between 200 mm and 300 mm [12]. Likewise, Neovision developed the Jetty robot for the inspection and cleaning of vertical ducts.

This system incorporates six tracked drive modules mounted on pantograph mechanisms, enabling the inspection of circular and rectangular ducts with diameters ranging from 400 mm to 1,300 mm when operating with its extended-arm configuration [13].

Moreover, developing control systems for mobile robots capable of adapting to pipelines with variable diameters remains a complex and contemporary engineering challenge. Reference [14] presents an analytical approach for a robotic system capable of adjusting its traction force while moving through pipelines with circular cross-sections only.

In 2018, [5] introduced a crawler-type inspection robot incorporating an active adaptation mechanism. This robot focused on modeling, simulation, and control for the inspection of pipelines and ducts with circular and rectangular cross-sections, whether horizontal or vertical, including curved sections and interconnections. However, the proposed system did not provide specifications regarding an integrated design process.

In summary, the existing literature reveals a limited number of studies addressing pipeline inspection systems supported by advanced autonomous control architectures capable of adapting to different pipeline diameters, cross-sectional geometries, and unconventional changes in direction (greater or less than 90°) [15], [16].

Several robotic platforms have been developed to occupy the entire internal diameter of the pipeline, adopting locomotion mechanisms inspired by biological organisms such as worms, snails, caterpillars, snakes, walking animals, and even flying species. Within this biomimetic perspective, the present research follows a bionic approach framed within the principles of sustainable innovation [17], using nature as a source of inspiration for solving engineering problems. Previous studies have primarily focused on the mathematical modeling of snake-like robot locomotion [3], [18], while others have investigated worm- or caterpillar-inspired robots equipped with wheels, climbing mechanisms, or obstacle-assisted locomotion for confined environments with different cross-sectional geometries and lengths. Additional studies have explored the locomotion of aquatic species, including whales and sharks [19]–[23]. However, to the best of the authors' knowledge, no previous research has addressed a robotic platform inspired by frog locomotion, reproducing its lateral undulations, forward progression, rectilinear displacement, and lateral movements through a geometric model integrated with a control system validated by motion patterns from both kinematic and dynamic perspectives.

Consequently, this paper presents the development of the PhylloT PIG-type robot, designed to completely occupy pipelines with different geometric configurations. The proposed design is inspired by the biomechanics of the Colombian poison dart frog, *Phyllobates terribilis*, whose locomotion serves as the basis for reproducing three fundamental movement modes: linear, rotational, and angular. The research includes kinematic and dynamic analyses, motion prediction, and geometric modeling within a parameterized CAD-based virtual environment, together with the corresponding control model implemented in MATLAB®. The primary objective is to provide an innovative methodology validated through mathematical, geometric, and physical modeling while effectively integrating computational design and simulation tools.

The remainder of this paper is organized as follows. First, the theoretical background and the mathematical notation underlying the simulation and control models are presented. Next, the materials employed for the study and implementation are described. The methodology is then divided into three stages: (i) geometric design and parameterization in SolidWorks®; (ii) transition from the CAD environment to the virtual control model through Simscape Multibody®; and (iii) control simulation using Simulink® in MATLAB®, including position validation without physical sensors using SolidWorks® Motion. Finally, the results, discussion, and conclusions are presented [20].

2. BACKGROUND AND MATHEMATICAL MODEL NOTATION

Simulation constitutes a fundamental tool for synthesizing the control laws governing robotic solutions for pipeline inspection through the virtualization of a geometrically modeled robotic platform. The simulation model is considered valid provided that its behavior accurately approximates the real operating behavior of the robot during pipeline inspection. Consequently, the dynamic and kinematic behavior of PhylloT is modeled using Hybrid Differential-Algebraic Equations (HDAEs) [21], requiring computational tools capable of solving these equations through appropriate numerical techniques [22].

The kinematic model describes the robot's velocities in Cartesian terms as a function of the velocities of *PhylloT's* components [23]. It also includes PhylloT's geometric information for its mechanical design and plant development. Furthermore, it allows the Cartesian position of any element to be expressed, making it the foundation for designing controllers [24]. The direct kinematic model is defined by expression (1): $\dot{X} = J\,(q).q$ (1); where $\dot{X} \in R^6$ is a vector containing the robot's linear and angular velocities; $J(q) \in R^{6xn}$ is the Jacobian matrix; n represents the robot's degrees of freedom, and $q \in R^n$ is the vector of positions of the robot's components.

The inverse kinematic model follows expression (2): $q = J^{-1}(q).\ \dot{X}$ (2). Trajectories, positions, velocities, and trajectory interpolation are determined using both the direct and inverse kinematic models [25].

On the other hand, the dynamic model contains all the geometric and dynamic information about *PhylloT* and is expressed by (3): $\gamma = f(q, \dot{q}, \ddot{q})$ (3). Where γ is the vector containing the torques of each element of *PhylloT* [26], q is the vector of generalized positions, and $q, \dot{q}, \ddot{q} = f(q, \dot{q}, \gamma)$ (4) [29].

2.1. MATHEMATICAL MODELING FOR CONTROL, [27]

In this case, the modelling starts with an electromechanical transducer defined as a device that transforms electrical energy into mechanical energy and vice versa. This is described by equation (5): $V_A(t) = R_A i(t)_A + L_A \frac{di(t)_A}{dt} + v(t)_g$ (5); where $V_A(t)$ is the voltage applied to the terminals of the armature; L_A and R_A are the inductance and resistance of the armature, respectively; $i(t)_A$ is the circulating current. The mechanical block of the gear motor is then modeled, defined as a compact mechanical device whose main function is to reduce the motor's rotational speed while increasing torque [28]. The modeling is described by equations (6)-(10):

$$T_M = T_i + T_r \quad (6);$$

$$T_i = \alpha(t)Ki = Ki\frac{d^2\theta(t)}{dt^2} \quad (7);\quad T_r = w(t)Kr = Kr\frac{d\theta(t)}{dt^2} \quad (8);$$

$$w(t) = \frac{d\theta_{(t)}}{dt} \quad (9);\quad \alpha(t) = \frac{dw_{(t)}}{dt} = \frac{d^2\theta(t)}{dt^2} \quad (10);$$

where $\theta(t)$ represents the angles traversed through the magnetic flux; the force $°F$ is proportional to the intensity of the magnetic field B, and the length of the coil or conductor L; and $T_M(t)°$ is the resulting torque that causes the rotor to rotate. For a linear analysis, it is necessary to assume that this torque or moment is proportional to the magnetic flux $\theta(t)°$ and the armature current $i(t)_A$, [32].

Regarding the mechanical block of the cylinder, it is defined as a mechanism that prevents undesired movement of the rod (or plunger) of a hydraulic or pneumatic cylinder, ensuring it remains in a specific position even if fluid pressure decreases or is interrupted [30].

In equation (12): $T_m = K_I\frac{d^2\theta(t)}{dt^2} + K_I\frac{d\theta_{(t)}}{dt}$ (12), Rotational motion is described, where T_m represents the torque, M the moment of inertia, K he angular stiffness constant, $\theta(t)$ the angle of rotation as a function of time, and $\frac{d^2\theta(t)}{dt^2}$, $\frac{d\theta_{(t)}}{dt}$, are the angular acceleration and angular velocity, respectively, of the linear motion. And equation (13): $F(T) = K_R\, d(T)$ (13), Describes linear motion, where $F(T)$ is the force as a function of time, K_R the linear stiffness constant, and $d(T)$ the deformation (or displacement) as a function of time [31].

Regarding trajectories, since sensors are not used, they are generated by tracking Cartesian coordinates of straight lines at a constant velocity. When the points of origin and destination are excessively distant, intermediate points must be selected to ensure that the control system adjusts not only to a specific control point but also to the trajectory indicated in the program. For this reason, linear interpolation is required, either through cubic splines, quintic splines, or segments composed of multiple parts [32].

2.2. MATHEMATICAL MODELING OF CONTROL [35]

According to equation (2), for *PhylloT*, it is assumed that using the kinematic model with system velocities is sufficient. In this case, a control scheme analogous to one developed with a dynamic and kinematic model is used, where position is controlled by considering an auxiliary control input and a calculated torque control. This transforms the problem from dynamic control to kinematic control through the following relationships (14)-(16): $\gamma = B_{-1}(q)\,[M(q)_u + V_m(q - q)_\eta]$ (14); $q^{\cdot} = S(q)_\eta$ (15); $\eta^{\cdot} = u$ (16)

These equations describe a dynamic system where γ is a function of q, u, and η; q is a state that changes over time, affected by $S(q)_\eta$; η is a state that changes over time and is driven by u.

The control development through Backstepping [33] is defined by equations (17) and (18): $\chi^{\cdot} = v_r \cos(\theta)$, $\gamma^{\cdot} = v_r \sin(\theta)$, $\theta_r = \varpi_r$ (17); $q_r = [\chi_r, \gamma_r, \theta_r]^T$ $V_r = [v_r, w_w]^T$ (18); These equations aim to achieve point-to-point trajectory tracking by considering reference velocities and positions. It is necessary to determine a control velocity (19): $V_C = f_c\,(e,\ V_r,\ k)$ such as $(q_r - q) = 0$ (19).

For tracking, equation (20) is used:

$$e = [e_1, e_2, e_3]^t = [\cos(\theta)\ \sin(\theta)\ 0,\ -\sin(\theta)\ \cos(\theta)\ 0,\ 0\ 0\ 1]^T$$

$= [\chi_r - \chi, \gamma_r - \gamma, \theta_r - \theta]^t$ (20); where e_1, e_2 are the positional errors relative to the moving reference frame $\{P_0, \chi_m, \gamma_m\}$, and the trajectory to follow is $q_r = \{\chi_r, \gamma_r, \theta_r\}^T$. The time derivative of the error takes the form of equation (21):

$$e' = [v^r = \cos(e_3) - w_r\, d\cos(r)\, \sin(e_3) - v_1 + v_2 e_2,\ v^r = \sin(e_3) - w_r\, d\cos(r)\, \cos(e_3) - v_2 + (d + e_1),\ w_r - v_2]^t \text{ (21)}.$$

The velocity of the center of mass is expressed in terms of $q_r = \{\chi_0,\ \gamma_0,\ \theta\}^T$; resulting in the dynamic model (22): $M_{(q)q^{\cdot}} + v_m\,(q, q^{\cdot})\, q^{\cdot} = \beta_{(q)}\Gamma - A^{\Gamma}(q)\,\tau$ (22).

Where:

$$M = \begin{bmatrix} m & 0 & -mdsin(\theta+\tau) \\ 0 & m & mdcos(\theta+\tau) \\ -mdsin(\theta+\tau) & mdcos(\theta+\tau) & md^2+l \end{bmatrix}$$

$$v_m = \begin{bmatrix} 0 & 0 & -mdcos(\theta+\tau)\theta'' \\ 0 & 0 & -mdsin(\theta+\tau)\theta' \\ 0 & 0 & 0 \end{bmatrix}$$

$$B = \frac{1}{r}\begin{bmatrix} cos\theta cos\theta \\ R - dsin(\tau)sin(\theta) \\ R - dsin(\tau) - R - dsin(\tau) \end{bmatrix}$$

$$A = [-sin(\theta)cos(\theta) \quad -dcos(\tau)] \qquad \tau = \begin{bmatrix} \tau_i \\ \tau_d \end{bmatrix}$$

v_r and ω_r are reference linear and angular velocities respectively, v_1 y v_2 belong to a control velocity vector: $v_c = [v_1 \;\; v_2]^T = [v \;\; w]^T$.

$$v_c = \begin{bmatrix} v_r \cos(e_3)\, w_r dcos(\tau)\sin(e_3) + k_x e_1 \\ w_r + v_r(k_y e_2 + k_\theta \sin(e_3)) \end{bmatrix} (23)$$ with k_x, k_y, k_θ as constants.

Equation (23) is developed from the Lyapunov function, incorporated to ensure its time derivative is strictly negative and to manage system uncertainty. The time derivative of (23) is expressed in equation (24):

$$v_c = \begin{bmatrix} \dot{v}_r \cos(e_3)\, \dot{w}_r dcos(\tau)\, sin(e_3) + k_x e_1 \\ \dot{w}_r + \dot{v}_r(k_y e_2 + k_\theta\, sin(e_3)) \end{bmatrix} +$$

$$\begin{bmatrix} k_x & 0 & v_r\, sin(e_3) & w_r dcos(\tau)cos(e_3) \\ 0 & v_r(K_r) & v_r\, K_\theta & cos(e_3) \end{bmatrix} e' \quad (24).$$

Throughout the model, it is assumed that the reference linear velocity v_r is strictly positive for $\forall\, t \geq 0$.

3. MATERIALS AND METHODOLOGY

As indicated in the Introduction, the proposed robot geometry is inspired by the morphology of an amphibian [34], specifically a frog characterized by a generally oval or elongated body and long, powerful hind limbs. Its anatomical structure, including the skeletal system, musculature, and skin, is directly related to its body shape and locomotion capabilities, particularly jumping and swimming. The design of the PhylloT robot assumes the locomotion behavior of a small frog navigating through a confined environment, taking as reference the inspection probes commonly used in pipelines and fittings, together with their architectural characteristics in terms of both form and function.

Accordingly, the robot incorporates angular motion through three or four anchoring points, uniformly distributed at angular separations of 120° and 90°, respectively, conceptually representing a dart frog with three or four limbs. The body geometry is simplified through its decomposition into elementary trapezoidal sections, facilitating the generation of the robot morphology and the positioning of the actuators, including both linear and rotary motors, as illustrated in Figure 4 [35].

Figure 4. Three-colored dart frog rendered for plant manufacturing or functional prototype in SolidWorks®.
Source: Own work

Regarding pipelines, networks, frameworks, and fittings, cylindrical pipes are considered, used to connect and direct materials [37] or flows. These include elbows, T-joints, crosses, reducers, flanges, plugs, and adapters; functional for connections and adjustments depending on the type of pipeline and the movement environment [6][39], see Figures 5 and 6.

Regarding *PhylloT's* movements, three are assumed in *SolidWorks® Motion®*: a linear movement, defined by the diameters of the pipes it inspects; a rotational movement, allowing it to navigate different locations; and an angular movement, enabling it to traverse within pipelines with branches ranging from 45° to 90° [47][48].

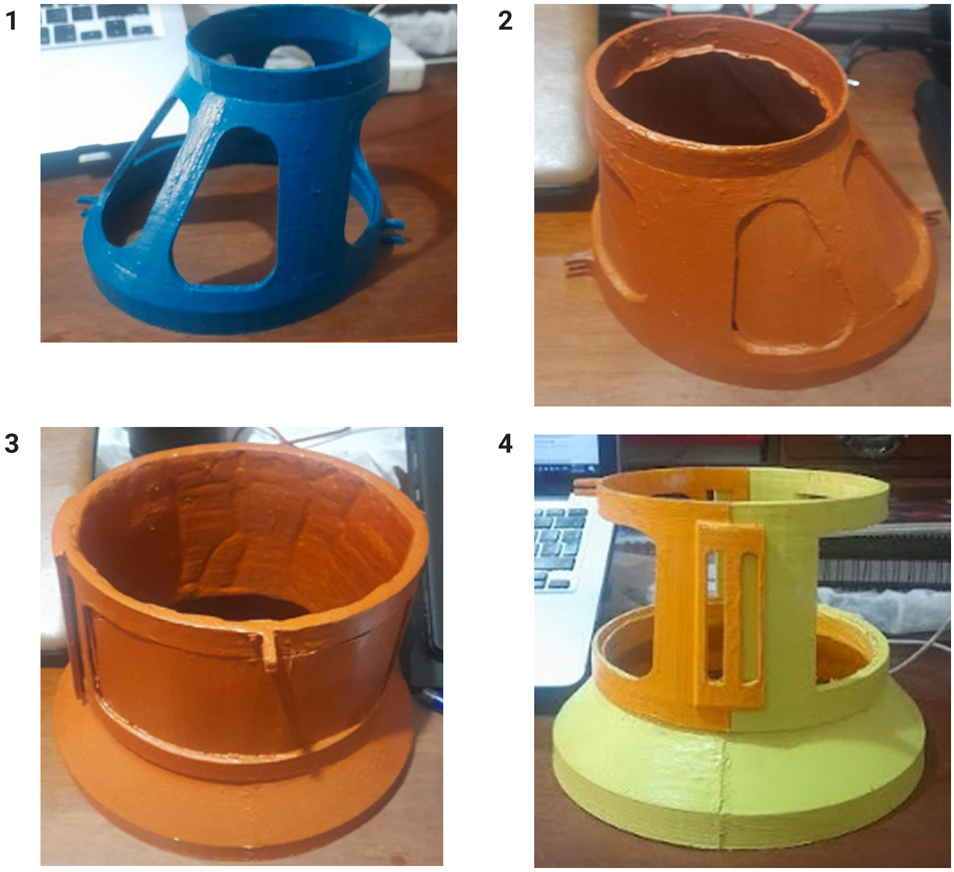

Figure 5. Eccentric reduction from 2” to 4”. Eccentric reduction from 4” to 6”, shifting the pipe axis [11]. Concentric branch or reduction from 4” to 6” [36]. Concentric branch or reduction from 6” to 8” that maintains the pipeline axis [39].

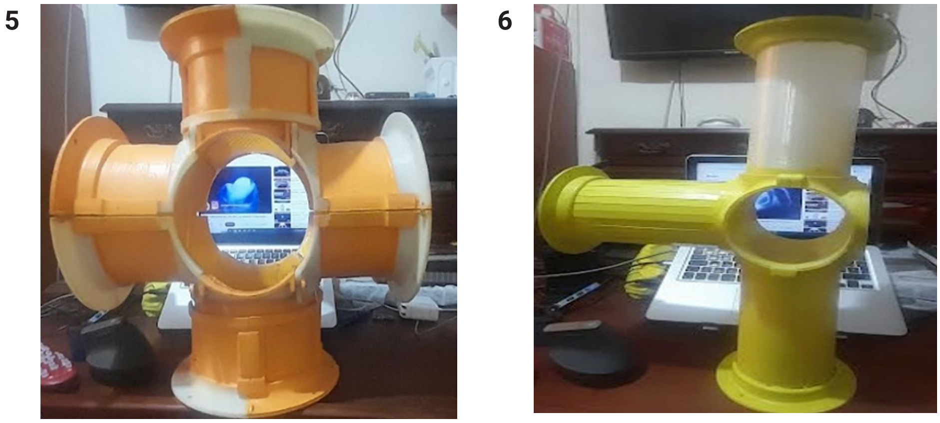

Figure 6. 5. Cross or 90-degree branch with a 6” diameter, requiring the robot to change its total position by 90° upward, downward, left, or right, or to continue forward without changing the angle. 6. Branch similar to the previous one, with a 4” diameter and a weld-able connector flange [36].

Source: Adapted from [40], own work

Methodologically, the initial stage comprised a review and analysis of the state of the art and previous studies [39], followed by the conceptual design and overall architecture of the PhylloT robot [38], including its morphology and locomotion strategy. Subsequently, the CAD model was developed and subjected to a matrix-based validation process to support the control model design [41].

The detailed design phase included three complementary components: (i) mechanical design, involving the development of engineering drawings for the mechanical parts while considering material selection, structural stresses, and manufacturing processes; (ii) electronic design, including the selection of sensors, actuators, and communication systems; and (iii) software development, encompassing the implementation of motion control, trajectory planning, and data processing algorithms [42].

Figure 7 presents the general block diagram of the proposed system. The robot, considered as the plant to be controlled, was initially developed through a conceptual design approach [43]. Subsequently, a CAD model was created using SolidWorks®, which served as the graphical environment for generating, modifying, and documenting two- and three-dimensional parts, assemblies, and engineering drawings [41], [44]. Finally, the complete model was exported to Simscape Multibody® and Simulink® in Matlab®, where the physical model and dynamic system were implemented using predefined blocks and simulation libraries [45], [46].

The development of the control model began with the definition of a pre-control plant and the controlled variable, namely the PhylloT robot position as a function of time, represented as a gray-box model based on the three locomotion modes previously described, as illustrated in Figure 9. For the implementation of the proportional control strategy and the selection of the actuators described in the mathematical model (6)–(10) and (12), both the linear and rotary motors were characterized [35]. Their corresponding geometries are presented in Figures 5 and 6.

The validation process focused on comparing the simulation results with the calibrated model and the input data implemented in Simscape Multibody® [47]–[49], using the Motion module available in SolidWorks®. Basic motion animations, dynamic simulations, and three-dimensional assembly motion analyses were performed. Subsequently, the motion of the assembly components was visualized and evaluated while considering physical properties, mass, gravitational effects, contact interactions, friction, and other dissipative phenomena [26], [47]. The analysis established position as the only independent variable, from which the corresponding velocity, acceleration, and displacement profiles of the PhylloT robot were obtained.

For linear trajectories, including angular trajectories discretized into 5° increments as control system inputs dependent on position and velocity according to

Equations (20) and (21), the corresponding paths are presented in Figure 8. The required number of wheel revolutions was calculated as 30,554 for Trajectory 1, 20,609 for Trajectory 2, and 354.9 for Trajectory 3. The wheel diameter used in the simulations was 0.44 m [48]–[51].

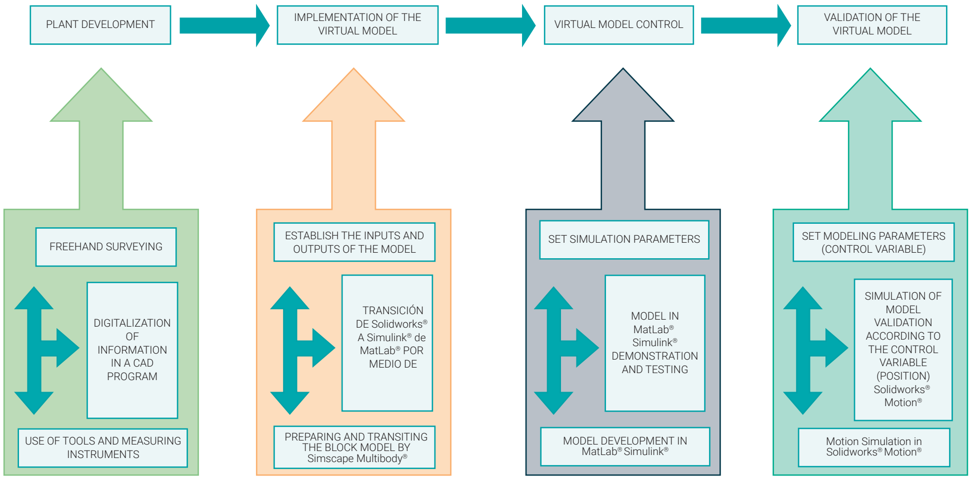

Figure 7. General block diagram.
Source: Own work

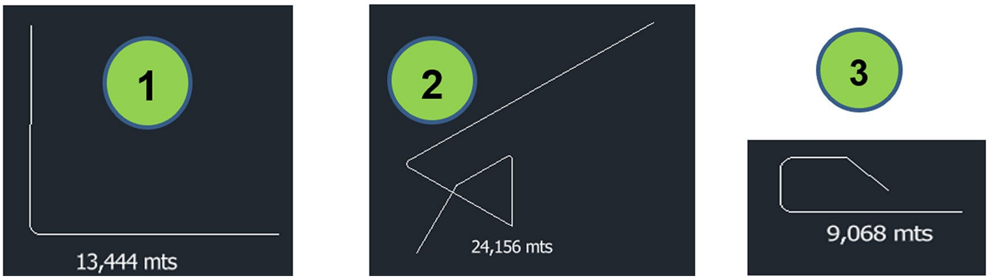

Figure 8. Trajectories 1, 2, and 3 to be evaluated, extracted from the environment (segments).
Source: Own elaboration (equations (14)-(17)).

4. RESULTS [45], [49].

4.1 Plant Generation for Virtualization

The virtualization of the plant and the environment (pipeline segment), complemented by images of the models created in *SolidWorks®* and exported to *DWG* format in *AutoCAD®*, is shown in Figure 9. The 90-degree pipe cut, and the linear motion and rotation (angles) mode are depicted in Figure 10 and the incorporated table [50]-[53]. The plant is presented in its front and rear views of the 3- and 4-point anchoring heads, as well as a side view, in Figures 6-8 [54], with actual dimensions. The physical properties of the plant, obtained from *SolidWorks®*, are generated through the program›s design platform [55].

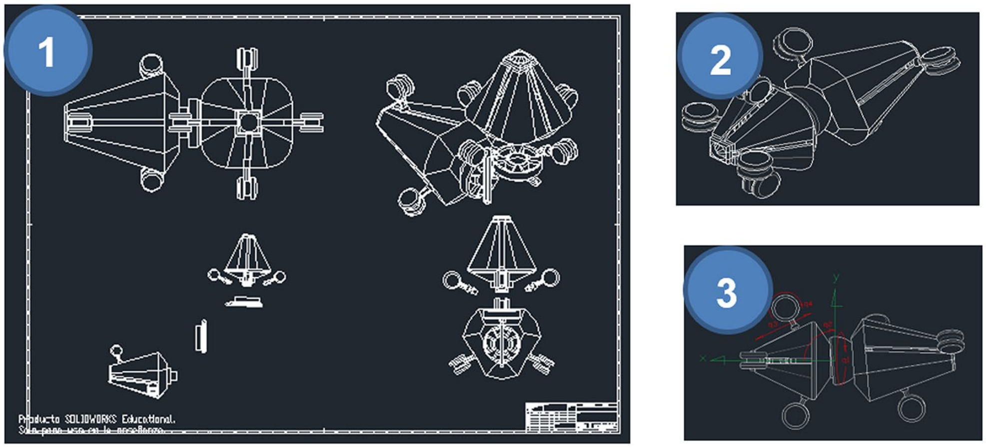

Figure 9. 1. Prototype images with three degrees of freedom and the environment, captured in DWG format [56]. 2. Isometric view; 3. Exploded view of the PhylloT robot, designed in AutoCAD®.
Source: Own elaboration [50][51].

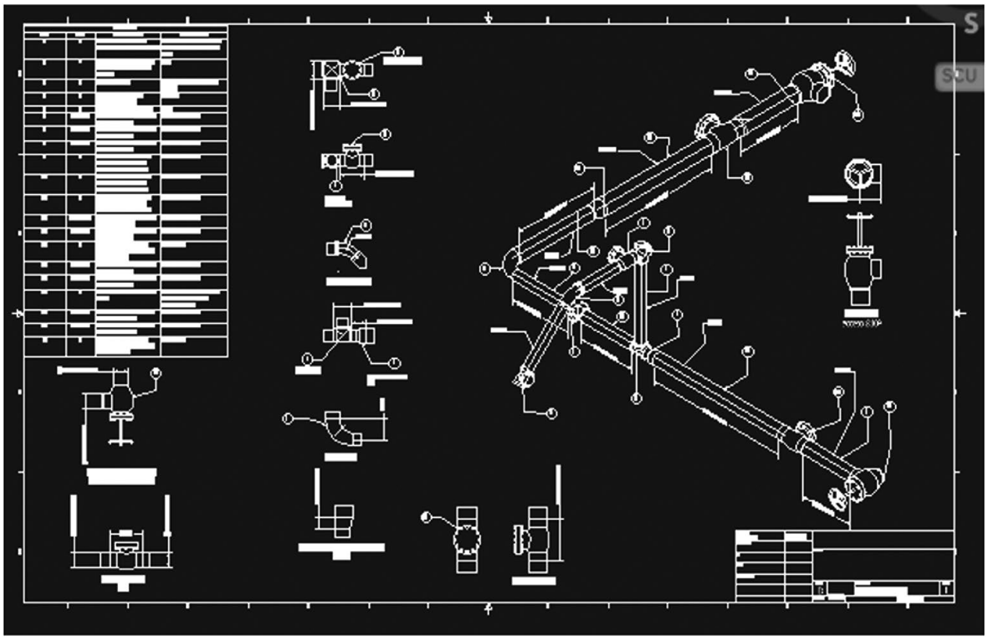

Figure 10. Isometric view and element table, designed in AutoCAD®.
Source: Own elaboration based on [52]. Equations (20)-(23).

4.2. SolidWorks® Model of PhylloT: Plant Design and Virtualization [3], [53]

The result involves the environment and two paths—pipes, segments—within the plant. The dimensions generated in *SolidWorks®* are shown in Figure 11.

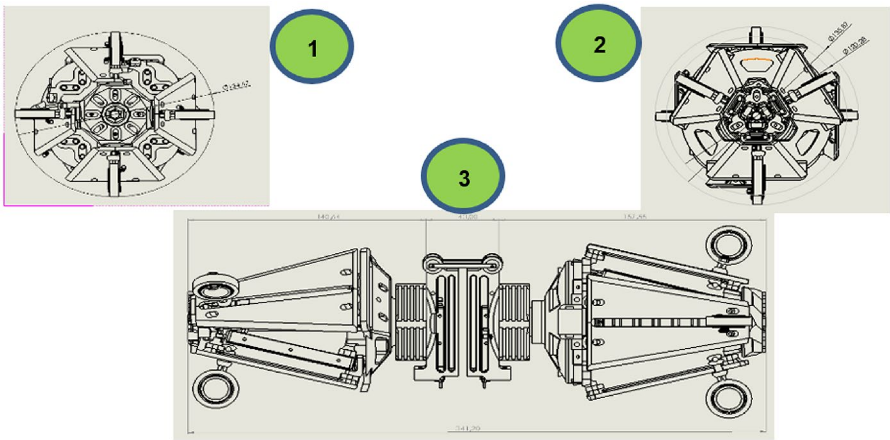

Figure 11. General dimensions generated in SolidWorks®: 4-anchor head, 3-anchor head, General plant.
Source: Own work

The physical properties of the plant obtained from *SolidWorks®* are shown in Figure 12. When incorporated into the configuration, they ensure the robot›s stability and maneuverability in alignment with the analytical expressions of the model (5)-(13).

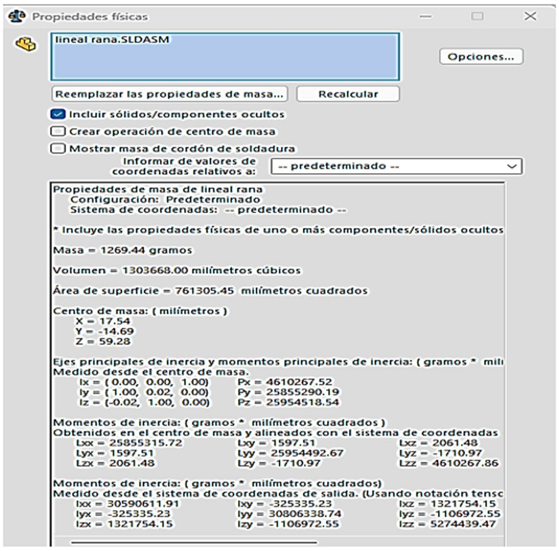

Figure 12. Physical elements of the PhylloT robot.
Source: Own elaboration (screenshot from SolidWorks®) [56].

a. Controller, [57].

For rotational freedom characteristics, the servos used—linear and continuous rotation, equipped with gears and pinions for executing complex tasks—were virtually modeled for *PhylloT*. They were equipped with position and velocity sensors to facilitate the execution of a Proportional Integral Derivative (PID) Control [57]. This approach increases the efficiency of the plant, although it is dimensionally scaled. The control is applied to the direction and rotation speed, not to a fixed position. The control block developed for system manipulation in *MatLab*® is shown in Figure 13. The controller aligns with the expressions (14)-(24) of the model.

The virtual system obtained simulates the machine and the motor speed of the wheel traction mechanism in full operation [69]. Therefore, it is divided into the three movements described in the methodology [49].

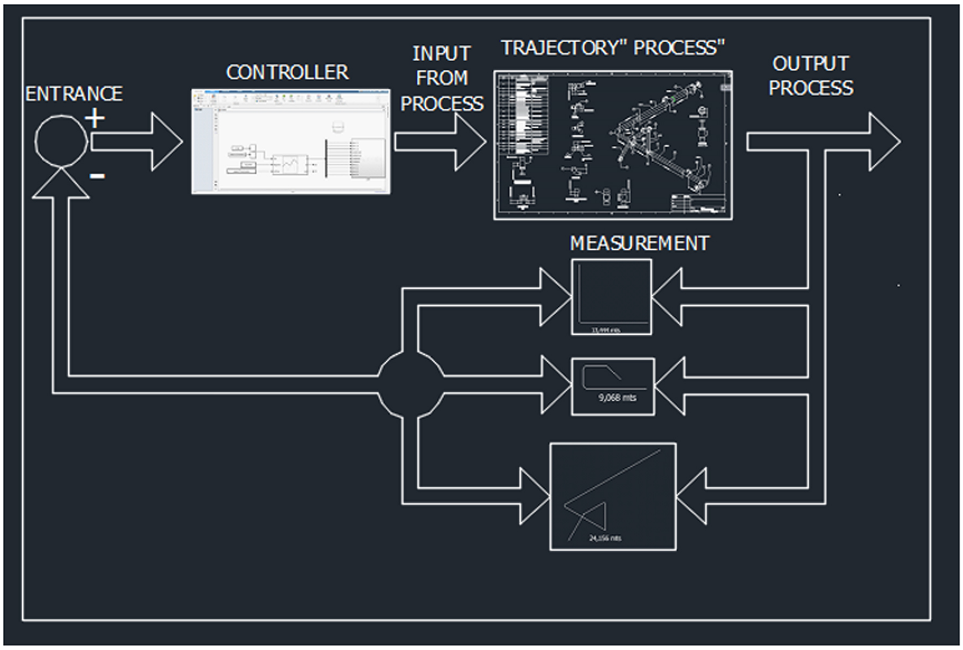

Figure 13. Closed-loop control block image, where the controller is modeled to integrate SolidWorks® and MatLab® to develop PhylloT for branching processes with three trajectories.

Source: Own elaboration adapted from [58]-[59].

For position control evaluation [62][64], Figure 9-3 is used. It features two 4” entry heads without rotation for elbows or reductions [60].

In Figure 14, the plant is shown at 90° as per Figures 6-5,6. Position changes for 6” piping are highlighted [63]-[66]—linear—but the initial angle changes due to the presence of an elbow. Similarly, lateral entry from left to right is also represented [68].

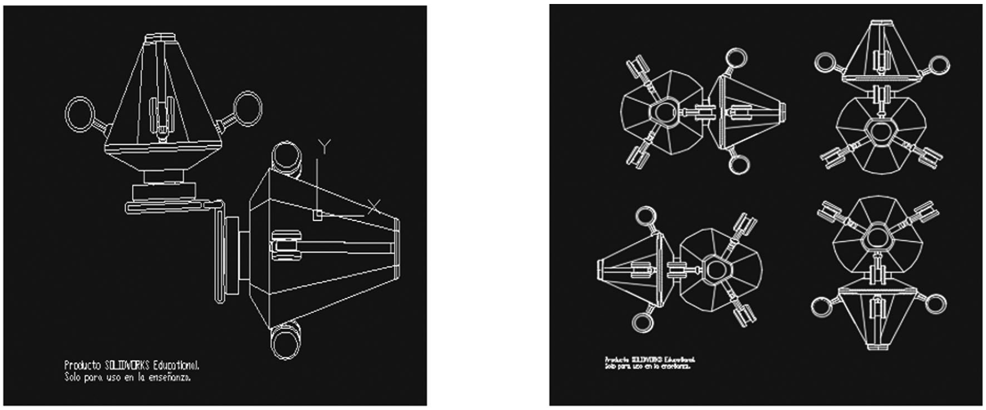

Figure 14. Position changes for inspecting 6” piping at 90° and possible rotations: linear, initial angle change, and lateral entry.
Source: Own elaboration [64].

b. Tool Assembly Protocol

The central focus of the simulation is the correct importation of the tool assembly and the validation of the PhylloT model from SolidWorks® [40] into Simscape Multibody®, and subsequently into Matlab® Simulink® [21], [60]. Therefore, both processes are described in detail below.

Initially, SolidWorks® must be configured to enable the export of files to Simscape Multibody® for subsequent integration into Matlab® [44].

After opening Simulink®, the corresponding Matlab® version (Win64) is specified, and the *Install Simscape Multibody® Link* interface is accessed [44]. In Step 1, the installation files are obtained by selecting *Get the Installation Files*.

Once the CAD design has been completed, the Simscape Multibody® export tools are accessed through *Link Export → Simscape Multibody®* [61]–[63]. The exported files are saved in a previously created folder to be imported into Matlab®. Running Matlab® with administrator privileges, the project folder is located, right-clicked, and the option *Remove from Path → Selected Folders* is selected. Subsequently, the command smimport is executed using the corresponding XML file generated by SolidWorks® (in this case, *rana lineal matlab.xml*), followed by pressing **Enter**.

Next, the Matlab® institutional license credentials are entered, including the registered email address, postal code, and license year. The appropriate version of Simscape Multibody® is then selected according to the installed Matlab® release, the operating platform (Win64), and the corresponding Simulink® version (*.m). The installation files are stored in a separate preconfigured folder.

Subsequently, the project folder is opened in the Matlab® workspace. In the command window, the installation command `installaddon('smlink-"Matlab version"-win64.zip')` is executed. Before performing this step, SolidWorks® must be completely closed. After the installation is completed, the operating system is restarted, Matlab® is opened with administrator privileges, and the command `regmatlabserver` is executed by pressing **Enter**.

Finally, SolidWorks® is reopened, and the Simscape Multibody® add-in should appear in the *Add-Ins* menu, confirming the successful integration between both software platforms, as illustrated in Figure 15 [62].

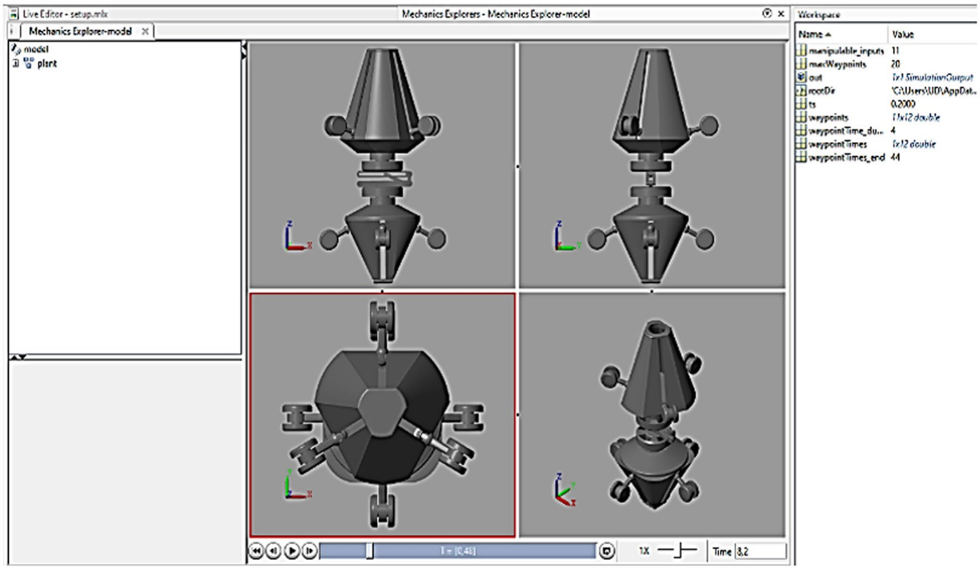

Figure 15. Plant exported to Simulink from SolidWorks [61].
Source: Own work

All subsystems can be identified: Total Assembly, Triple Head-Rotator-Quadruple Head; Triple Head; Rotator; and Quadruple Head. A, B, C, and D, respectively, in Figure 16.

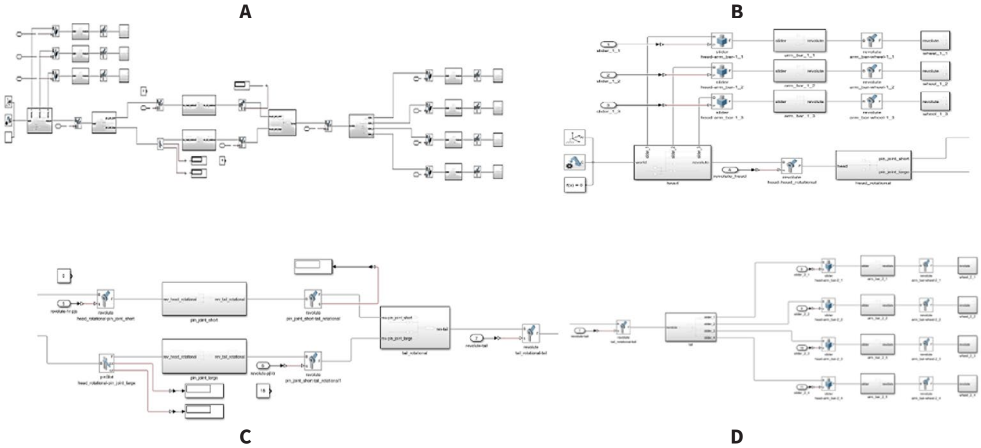

Figure 16. A. Total Assembly: Triple Head-Rotator-Quadruple Head; B. Triple Head; C. Rotator; D. Quadruple Head.

Finally, click "*Run*," resulting in a second screen displaying the *PhylloT* image [18]; see Figure 17.

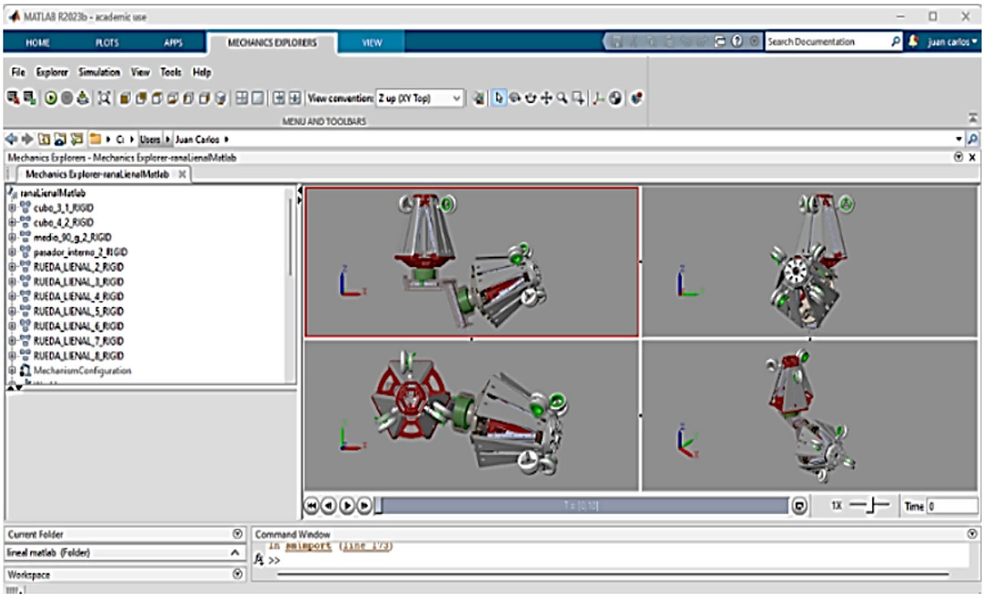

Figure 17. Final export.
Source: Own elaboration based on [68].

b. Matlab® Simulation

Following the transition described in Section 3.3, the control process begins by configuring the system inputs and the plant movements.

The execution sequence includes Slider-type inputs (1_1, 1_2, 1_3, and 2_1), Revolute-type inputs (head, hr, pjl, and tail), and the *Trapezoidal Velocity Profile Trajectory* block. Subsequently, the maximum number of waypoints is defined, an initial point is established in the XY plane, and a 12 × 12 matrix is configured. The matrix includes one input for 4", another for 5", and another for 6", while the remaining inputs correspond to angular positions of 135°, 90°, 90° rotation, 135°, 180°, 90°, 180°, 270°, and 360°, thereby defining a complete motion sequence.

c. Model Validation [67], [69]–[71]

The validation of the simulation model and the virtualization of the three- and four-point anchoring mechanisms were based on comparing the simulation results with those obtained from a calibrated model and the data extracted from the software tools. Although complete validation cannot be guaranteed, CAD software [63], based on the parameterization of real mechanical behavior and calibrated according to error measurements performed by the manufacturer (Dassault Systèmes), incorporates validation modules such as SolidWorks® Motion® [62], which provide reliable motion tracking and analysis.

Although position is the only independent variable, the system analysis considers linear displacement, rotational motion, and angular movement. Accordingly, the results obtained for each variable were processed using both SolidWorks® Motion® and the plant model.

1. **Resulting displacement in SolidWorks® Motion®:** PhylloT is positioned and anchored within the different pipeline diameters. The *Motion Analysis* module, located at the bottom of the SolidWorks® workspace tree, is then selected, specifying the linear motor edge velocity (24 mm/s in this study). Subsequently, all simulation data are exported to Microsoft Excel to generate the corresponding tables and equations for the kinematic variables, including velocity, acceleration, and displacement [71].
2. **Resulting displacement of the plant:** This stage consists of linear motion under proportional control for pipeline diameters ranging from 4" to 6" in increments of 0.25" (a minimum of eight intermediate positions), with a maximum of 127 discrete positions along the trajectory in SolidWorks® Motion® (one position per pre-control step) [62]. Level 1 of the plant analysis is divided into two stages: (i) three- or four-point anchoring, according to the architecture, geometry, and functionality of PhylloT; and (ii) evaluation of

pipeline branches and accessories, including concentric and eccentric reducers, as well as inclinations ranging from 0° to 90° in horizontal, vertical, and diagonal configurations, evaluated at 15° intervals.

For both displacement analyses, 126 frames were sampled over a 5 s interval for each of the six kinematic variables. The corresponding results are presented in Figures 18–20.

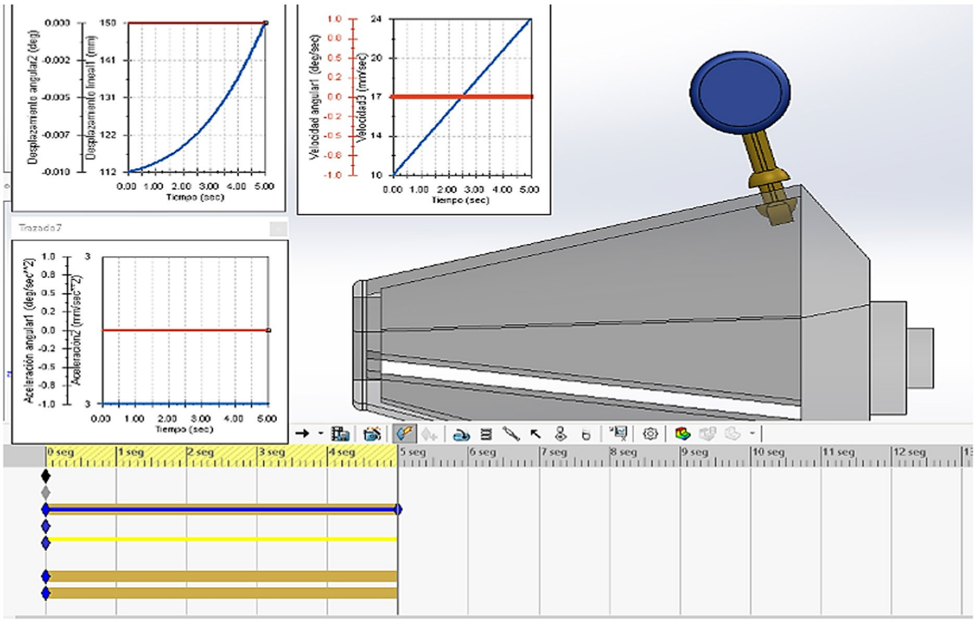

Figure 18. Graphs of Linear and Angular Displacement (left), Linear and Angular Velocity (top right), Linear and Angular Acceleration (bottom left); based on frames from SolidWorks® Motion®.

Source: Own work

For Figure 18, the following is indicated over a period of 600 seconds:

- **Linear and Angular Velocity:** A distance of 70 mm is covered by the 4-point anchor head in contact, and 10 mm by the 3-point anchor head in contact, recorded as $\frac{mm}{seg}$. The **linear velocity**, according to the position equation *y = 2,8x + 10*, is constant; the **angular velocity** is also constant, with the position equation y = *0*.
- **Linear and Angular Acceleration**: A distance of 70 mm is covered by the 4-point anchor head in contact, and 10 mm by the 3-point anchor head in contact, recorded as $\frac{mm}{seg^2}$. The **linear acceleration**, according to the

position equation *y = -9E-16x + 2,8*, is constant; the **angular acceleration**, according to the position equation *y = 0, is also constant.*

- **Linear and Angular Displacement:** Recorded in mm; the **linear displacement** follows the position equation *y = -3E-30x - 6E-15*; the **angular** displacement follows the position equation *y = 7,366x + 106,57.*

For rotation, selecting a rotational motor with 24 mm/sec, the graphs and position equation for each predefined variable are generated.

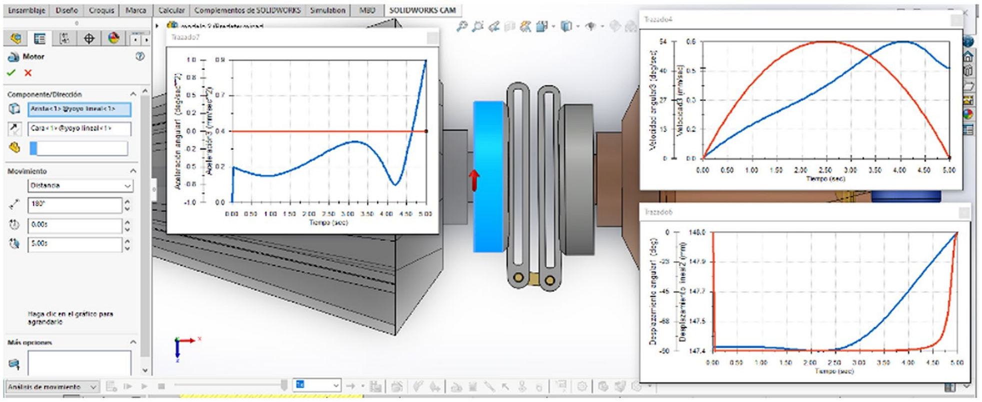

Figura 19. Para una Rotación proporcional: Aceleración Lineal y Angular (izq.), Velocidad Lineal y Angular (der. Arriba), Desplazamiento Lineal y Angular (der. Abajo); a partir de fotogramas de Motion® de SolidWorks®.
Fuente: elaboración propia.

For Figure 19, the following is indicated over a period of 600 seconds:

- **Linear Velocity:** Measured in $\frac{mm}{seg}$, with the position equation *y = 0,0459x + 35,651* ; **angular velocity** follows the equation *y = 0,1227x + 0,0624* at a 360° rotation.
- **Linear Acceleration:** Measured in $\frac{mm}{seg^2}$, with the position equation *y = 0,0576x + 0,1366* ; **angular acceleration** is constant, following the equation *y = 0.*
- **Linear Displacement:** Measured in mm, with the position equation *y = 0,1091x + 147,26*; **angular displacement** follows the equation *y = 3,3459x - 93,834.*

For an angle, selecting a rotational motor with 24 mm/sec; and based on an environmental study with pipelines inclined every 15 degrees—ranging from 0 to 90 degrees—the system allows for various degree-by-degree or fractional degree variations, as it is a proportional system.

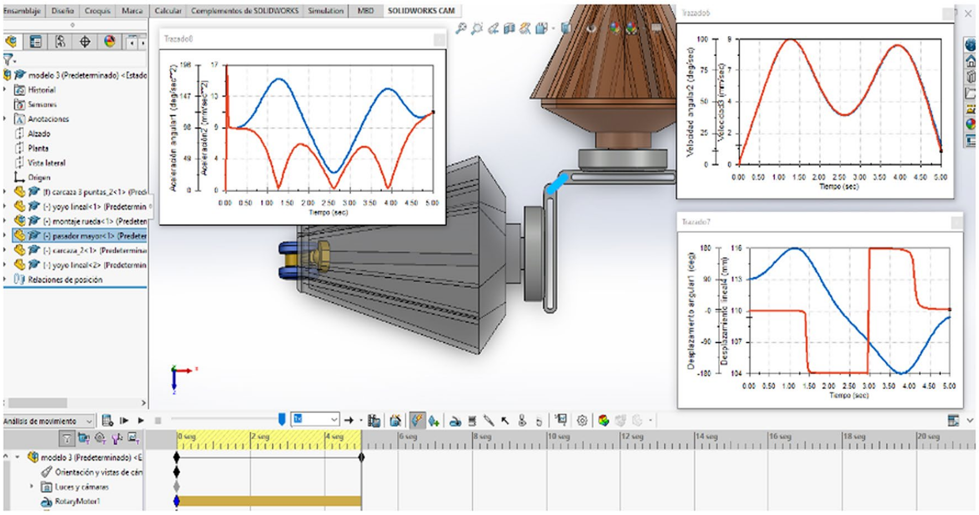

Figure 20. For a proportional angle: Linear and Angular Acceleration (left), Linear and Angular Velocity (top right), Linear and Angular Displacement (bottom right); based on frames from SolidWorks® Motion®.

Source: Own work

For Figure 20, the following is indicated over a period of 600 seconds:

- **Linear Velocity**: Measured in $\frac{mm}{seg}$, with the position equation *y=1.5491x+59.529y=1.5491x+59.529*; **angular velocity** follows the equation *y=0.1608x+5.1543y=0.1608x+5.1543*.
- **Linear Acceleration**: Measured in $\frac{mm}{seg^2}$, with the position equation *y=0.0298x+9.7337y=0.0298x+9.7337;* **angular acceleration** follows the equation *y=−0.837x+62.613y=−0.837x+62.613*.
- **Linear Displacement**: Measured in mm, with the position equation *y=−2.2199x+115.92y=−2.2199x+115.92;* **angular displacement** follows the equation *y=28.747x−85.689y=28.747x−85.689*.

5. DISCUSSION

The use of integrated software environments such as Matlab® and SolidWorks® for the design, simulation, and validation of robotic prototypes has become an increasingly common practice in engineering because it enables the evaluation of mechanical behavior and control strategies before physical implementation.

From one perspective, this approach offers significant advantages, including reductions in development time, implementation costs, engineering effort, and infrastructure requirements. Virtual prototyping allows multiple design iterations to be evaluated rapidly, facilitating the optimization of both mechanical configurations and control algorithms before manufacturing the physical prototype.

Conversely, some authors argue that numerical simulations cannot completely reproduce real operating conditions. The accuracy of simulation results depends directly on the completeness of the mathematical model, the quality of the geometric representation, and the fidelity with which the simulation reproduces the actual behavior of the prototype. Consequently, modeling errors or incorrect assumptions may remain undetected during the virtual design stage and subsequently be transferred to the final product. Similar situations have been reported in industrial developments, including failures identified during the development of commercial Intel® microprocessors.

Within the context of the present research, the integration of SolidWorks®, Simscape Multibody®, and Matlab® Simulink® enabled the complete simulation of the proposed robotic model. The virtual environment made it possible to analyze the robot's operating behavior, including linear displacement, rotational speed, and angular velocity, while validating the consistency of the mathematical model. The simulation results showed agreement with the expected mechanical behavior, confirming the adequacy of the proposed modeling and parameterization strategy for the virtual evaluation of the PhylloT robot.

6. CONCLUSIONS

This research presented the development of a virtual simulation model for the PhylloT robot by integrating SolidWorks®, Simscape Multibody®, and Matlab® Simulink®. The proposed framework enables three-dimensional virtual operation of the robot while combining CAD-based geometric modeling with dynamic simulation and automatic control. The mathematical model of the manipulator was validated using the SolidWorks® Motion® module.

The complete simulation required the implementation of both kinematic and dynamic models. The combined use of Matlab® and Simulink® allowed the verification of trajectories, positions, velocities, and accelerations under different operating conditions, demonstrating the suitability of the proposed methodology for robotic exploration and pipeline inspection applications.

The validation process, based on parameterized mechanical behavior and synchronized motion analysis, was performed using the SolidWorks® Motion® tracking module. This approach provided an effective mechanism for comparing the predicted behavior of the mathematical model with the simulated mechanical response.

The results presented in Figures 18–20 demonstrate that, during a 600 s simulation, using 126 sampled frames and a rotational motor speed of 24 mm/s, the system position—considered the primary control variable—maintained consistent functional relationships with the corresponding linear and angular velocities, accelerations, and displacements. The resulting curves were fully consistent with the parameterization implemented in SolidWorks®, confirming the suitability of the proposed methodology for supporting the analysis and future implementation of real pipeline inspection systems.

Although classical PID controllers are not necessarily the optimal solution for robotic position control, they provide an effective starting point for achieving rapid responses to control inputs. Consequently, the modular dynamic model developed for PhylloT establishes a suitable foundation for future research involving nonlinear, adaptive, and intelligent control strategies capable of improving disturbance rejection and overall system performance. These developments may be evaluated through computational simulations incorporating adaptive algorithms and artificial intelligence techniques.

Overall, the results demonstrate that designing, analyzing, and validating robotic prototypes within integrated virtual environments such as SolidWorks® and Matlab® constitutes an effective engineering methodology that significantly increases confidence in the functional design prior to physical implementation. This approach has the potential to reduce infrastructure requirements, development costs, and detailed engineering time for pipeline inspection systems, while also being applicable to other industrial scenarios, including hydroelectric generation systems [72].

Acknowledgments: The authors acknowledge the SciBas Research Group, the Eureka Research Group, affiliated with the Research Office of Universidad Distrital Francisco José de Caldas, and the Biodiversity for Society Research Group at Universidad Nacional de Colombia, La Paz Campus.

REFERENCES

[1] T. Zlateva and G. Tuparov, Eds., Computer Science and Education in Computer Science: 19th EAI International Conference, CSECS 2023, Boston, MA, USA, June 28–29, 2023, Proceedings, vol. 514, Lecture Notes of the Institute for Computer Sciences, Social Informatics and Telecommunications Engineering. Cham, Switzerland: Springer, 2023, pp. 247–262, doi: https://doi.org/10.1007/978-3-031-44668-9.

[2] S. Banna and S. Steephen, "A review on various in-pipe inspection methods for a pipeline," in Proc. Int. Conf. Power, Instrumentation, Control and Computing (PICC), Thrissur, India, Apr. 2023, pp. 1–5, doi: https://doi.org/10.1109/PICC57976.2023.10142798.

[3] J. Vrana, N. G. Meyendorf, N. Ida, and R. Singh, "Introduction to NDE 4.0," in NDE 4.0 for Smart Inspection, Cham, Switzerland: Springer, 2021, pp. 1–28, doi: https://doi.org/10.1007/978-3-030-48200-8_43-1.

[4] Emerson, Rosemount™ PDS42 Acoustic Pig Detector: Product Data Sheet MS-00813-0209-3636, Aug. 2024. [Online]. Available: https://www.emerson.com/documents/automation/gu%EDa-de-inicio-r%E1pido-detector-de-pig-ac%FAstico-rosemount-pds42-es-11764116.pdf

[5] J. Liu, M. Li, Y. Wang, D. Zhao, and R. Deng, "Multi-gait snake robot for inspecting inner wall of a pipeline," Biomimetic Intelligence and Robotics, vol. 4, Art. no. 100156, pp. 1–10, 2024, doi: https://doi.org/10.1016/j.birob.2024.100156.

[6] M. Ciszewski, T. Buratowski, M. Giergiel, P. Małka, and K. Kurc, "Virtual prototyping, design and analysis of an in-pipe inspection mobile robot," Journal of Theoretical and Applied Mechanics, vol. 52, no. 2, pp. 417–429, 2014.

[7] A. Lamas, "Robot inspeccionador de tuberías," M.S. thesis, Máster Univ. Ingeniería Mecatrónica, 2017. [Online]. Available: http://hdl.handle.net/10651/43580

[8] ABE Group, "Kamery inspekcyjne do kanalizacji – Precyzyjna diagnostyka rur i przewodów." [Online]. Available: https://www.abekamery.pl/

[9] C. A. García, "Palpador mecánico para robot de inspección de tuberías," M.S. thesis, Universidad Nacional de Colombia. [Online]. Available: https://repositorio.unal.edu.co/handle/unal/70385

[10] J. Colorado, D. Patiño, F. Ruiz, L. Solaque, R. Duarte, and F. J. Sichaca, "Dispositivo para la exploración y/o reparación de tuberías con dispositivos de detección de imágenes y/o mecanismo de desbaste o pulido y/o mecanismo de reparación," Colombian Patent NC2019/0009551.

[11] VAM Industry, "Tuberías, válvulas y accesorios." [Online]. Available: https://ddd.uab.cat/pub/tfg/2016/148700/TFG_VamIndustry_v04.pdf

[12] D. Beciri, "Neovision Jetty robot uses dry ice blasting for air duct cleaning." [Online]. Available: https://www.robaid.com/robotics/neovision-jetty-robot-uses-dry-ice-blasting-for-air-duct-cleaning.htm

[13] R. Raj and A. Kos, “A comprehensive study of mobile robots: History, developments, applications, and future research perspectives,” Applied Sciences, vol. 12, no. 14, Art. no. 6951, pp. 1–26, 2022, doi: https://doi.org/10.3390/app12146951.

[14] J. De França Freire, M. R. Rennó Gomez, and M. Guedes Gomes, “Pipeline inspection,” in Handbook of Pipeline Engineering. Cham, Switzerland: Springer, 2024, pp. 35–36, doi: https://doi.org/10.1007/978-3-031-33328-6.

[15] J. L. Andrade, H. Romero Rodríguez, J. J. Rodríguez Castaño, F. J. Pérez Grau, J. Carpes Hortal, and A. Ollero Baturone, “Diseño y desarrollo de un robot aéreo para la inspección de colectores de saneamiento,” in XLI Jornadas de Automática, Ferrol, Spain, 2019, pp. 647–654, doi: https://doi.org/10.17979/spudc.9788497497169.647.

[16] A. F. Segovia-Razo, “Diseño e implementación de un robot móvil con un sistema de sensores inteligentes para la detección de fallas en tuberías primarias de Lima Norte,” B.S. thesis, 2021. [Online]. Available: http://hdl.handle.net/20.500.12404/20198

[17] J. J. Escobar-Kögler, “Biorrobótica: Intersección entre la biología y la robótica,” Universidad Mariano Gálvez, Oct. 2023, doi: https://doi.org/10.13140/RG.2.2.24112.94724.

[18] R. Ñiquen, “Diseño mecánico y análisis cinemático de un robot reconfigurable para labores de rescate ante un inminente terremoto,” B.S. thesis, Universidad de Ingeniería y Tecnología, Lima, Peru, 2021, pp. 26–39. [Online]. Available: https://repositorio.utec.edu.pe/handle/20.500.12815/261

[19] H. Ryeol and S. Roh, “In-pipe robot with active steering capability for moving inside of pipelines,” in Bioinspiration and Robotics: Walking and Climbing Robots. Rijeka, Croatia: InTech, 2007, pp. 375–402, doi: https://doi.org/10.5772/5512.

[20] E. Lugo-González, A. Velarde-Galván, and M. Arias-Montiell, “Mechatronic design implemented in the development of virtual and physical prototypes,” in Handbook of Research on Mechatronics Engineering, pp. 22–39, 2020, doi: https://doi.org/10.35429/H.2020.5.22.39.

[21] V. H. Mosquera-Leyton and O. A. Vivas-Albán, “Control backstepping de un robot SCARA con incertidumbre paramétrica,” Ciencia e Ingeniería Neogranadina, vol. 22, no. 1, pp. 107–122, Jan. 2012, doi: https://doi.org/10.18359/rcin.252.

[22] E. Cardoso, A. Fernández, S. Marrero-Osorio, and P. Guardado, “Kinematic and dynamic models for a 4-DOF robot,” RIELAC, vol. 38, no. 3, pp. 56–75, Sep.–Dec. 2017. [Online]. Available: http://scielo.sld.cu/pdf/eac/v38n3/eac06317.pdf

[23] K. Ramírez Benavides, "Cinemática directa del robot." [Online]. Available: https://www.kramirez.net/Robotica/Material/Presentaciones/CinematicaDirectaRobot.pdf

[24] J. C. Corredor-Carreño and O. A. Gonzales-Triana, "Diseño de un controlador adaptativo basado en los parámetros de sintonización de Ziegler y Nichols para plantas de primer orden," B.S. thesis, Fundación Universitaria Los Libertadores, Bogotá, Colombia, 2012. [Online]. Available: http://hdl.handle.net/11371/4720

[25] Iris Dynamics, "Forward and inverse kinematics: Explained." [Online]. Available: https://irisdynamics.com/articles/forward-and-inverse-kinematics

[26] J. C. Rodríguez-Zambrana, "Modelo cinemático y control de un brazo robótico imprimible," B.S. thesis, Universidad Carlos III de Madrid, Madrid, Spain. [Online]. Available: https://core.ac.uk/download/29404184.pdf

[27] R. Torrealba, A. Clavijo, and M. Delgado, "Modelaje matemático y simulación de un robot manipulador de microprocesadores: Dos enfoques," Revista de la Facultad de Ingeniería UCV, vol. 21, no. 3, pp. 121–139, Sep. 2006.

[28] B. A. Falcon Mendoza, Á. S. Velásquez Benavidez, D. R. Ñacato Estrella, F. J. Santacruz Sulca, and D. F. Veloz Cherres, "Modelado matemático, simulación e implementación de pruebas en un motor DC LabVolt," Polo del Conocimiento, vol. 7, no. 7, pp. 997–1018, Jul. 2022.

[29] Advanced Motion Controls, "¿Qué es el servomecanismo? Definición de servosistemas, historia, componentes y aplicaciones," Aug. 2024. [Online]. Available: https://www.a-m-c.com/es/servomecanismo/

[30] T. Szakács, "A MATLAB/Simulink® dynamic model of a pneumatic piston and system for industrial application," in Proc. 4th Int. Symp. Multidisciplinary Studies and Innovative Technologies (ISMSIT), 2020, pp. 1–8, doi: https://doi.org/10.1109/ISMSIT50672.2020.9255177.

[31] L. A. García-Delgado, "Control de robots manipuladores 04: Cinemática de velocidad—El jacobiano," Nov. 2020. [Online]. Available: https://sivea.uson.mx/Docentes/Tareas/Presentacion_U4_Robots.pdf

[32] O. A. García-Campos, "Modelado, simulación y control de un quadrotor para transporte de carga colgante: Extensión al caso tridimensional," B.S. thesis, Escuela Técnica Superior de Ingeniería, Universidad de Sevilla, Sevilla, Spain, 2017. [Online]. Available: https://ereding.etsi.us.es/bibing/proyectos/use/abreproy/60409/fichero/PFCAlfredo.pdf

[33] P. Dourmashkin, "Angular velocity and angular acceleration." [Online]. Available: https://phys.libretexts.org/Bookshelves/Classical_Mechanics/Classical_Mechanics_(Dourmashkin)/06%3A_Circular_Motion/6.05%3A_Angular_Velocity_and_Angular_Acceleration

[34] GeeksforGeeks, "Morphology and anatomy of frogs." [Online]. Available: https://www.geeksforgeeks.org/frog-morphology/

[35] J. L. Fernández, "Momento lineal." [Online]. Available: https://www.fisicalab.com/apartado/cantidad-movimiento

[36] N. S. Chuquín-Vasco, J. P. Chuquín-Vasco, and D. A. Chuquín-Vasco, Hidráulica en tuberías y accesorios (válvulas industriales): Pérdidas, casos reales de aplicación y selección de bombas centrífugas. Riobamba, Ecuador: Escuela Superior Politécnica de Chimborazo, Grupo de Investigación en Seguridad, Ambiente e Ingeniería (GISAI), 2022. [Online]. Available: http://cimogsys.espoch.edu.ec/direccion-publicaciones/public/docs/books/2022-11-07-135357-LIBRO%20HIDRAULICA%20EN%20TUBERIAS%20Y%20ACCESORIOS.pdf

[37] U.S. Pipe, "Ductile Iron Pipe Product Brochure." [Online]. Available: https://uspipe.com/wp-content/uploads/2020/12/20111041547130.Ductile-Iron-FPF-SPN-Metric-BRO-089sm.pdf

[38] C. Tamara, E. Gambao, A. Brunete, and M. Hernando, "Micro-robot para inspección de tuberías," in Actas de las XXXVII Jornadas de Automática, 2016, pp. 683–688, doi: https://doi.org/10.17979/spudc.9788497498081.0683.

[39] J. S. Cortés-Quintero, "Desarrollo de un procedimiento de inspección para las tuberías de una planta de licuefacción de gas mediante ultrasonido multielemento de bajo perfil con focalización de elevación optimizada," B.S. thesis, Universidad Tecnológica de Pereira, Pereira, Colombia, 2023. [Online]. Available: https://repositorio.utp.edu.co/server/api/core/bitstreams/521b9937-a055-4641-bfea-d6dc16124d93/content

[40] J. Arciniegas Villamizar, L. A. Quintero, and J. Meneses Fonseca, "Análisis de técnicas de inspección no destructiva en tubería flexible con refuerzo no metálico para el transporte de hidrocarburos," Revista Colombiana de Materiales, no. 5, Special Issue, pp. 78–85. [Online]. Available: https://www.academia.edu/61436306/An%C3%A1lisis_De_T%C3%A9cnicas_De_Inspecci%C3%B3n_No_Destructiva_en_Tuber%C3%ADa_Flexible_Con_Refuerzo_No_Met%C3%A1lico_Para_El_Transporte_De_Hidrocarburos

[41] S. Jatsun, B. Lushnikov, O. Emelyanova, and A. Leon, "Synthesis of SimMechanics model of quadcopter using SolidWorks CAD translator function," in Proc. 15th Int. Conf. Electromechanics and Robotics (Zavalishin's Readings), vol. 187, Smart Innovation, Systems and Technologies, Singapore: Springer, 2021, pp. 125–137, doi: https://doi.org/10.1007/978-981-15-5580-0_10.

[42] Autodesk, "3D modeling software." Accessed: May 13, 2025. [Online]. Available: https://www.autodesk.com/latam/solutions/3d-modeling-software

[43] S. Arévalo-Fernández, "Aplicación de Simulink® y MATLAB® para análisis cinemático y dinámico, control y comunicaciones de robots industriales," B.S. thesis, Dept. Ingeniería de Sistemas y Automática, Universidad de Valladolid, Valladolid, Spain, Jun. 2020. [Online]. Available: https://uvadoc.uva.es/bitstream/handle/10324/47727/TFG-I-1889.pdf

[44] A. Herreros-López, "Proyecto SimRobots: Colaboración entre Simscape Multibody™ y Robotics System Toolbox™," in Actas de las XLV Jornadas de Automática, 2024, pp. 1–7, doi: https://doi.org/10.17979/ja-cea.2024.45.10770.

[45] L. Engelhardt, M. Burger, and G. Bitsch, "Real-time simulation of multibody systems for on-board applications," in Proc. 1st Joint Int. Conf. Multibody System Dynamics, Lappeenranta, Finland, May 2010. [Online]. Available: https://d-nb.info/1027389856/34

[46] R. Moreno-Cobos, "Modelado y simulación con CATIA V5® de operaciones de mecanizado en un torno paralelo," B.S. thesis, Escuela Técnica Superior de Ingeniería, Universidad de Sevilla, Sevilla, Spain, 2014. [Online]. Available: https://ereding.etsi.us.es/bibing/proyectos/use/abreproy/60204/fichero/Modelado+y+simulación+con+Catia+v5+de+operaciones+de+mecanizado+en+un+torno+paralelo.pdf

[47] D. Cekus, B. Posiadała, and P. Waryś, "Integration of modeling in SOLIDWORKS® and MATLAB®/Simulink® environments," Archive of Mechanical Engineering, vol. 61, no. 1, pp. 3–18, 2014, doi: https://doi.org/10.2478/meceng-2014-0003.

[48] D. Xue and Y. Chen, *System Simulation Techniques with MATLAB® and Simulink®*. Hoboken, NJ, USA: John Wiley & Sons. [Online]. Available: https://www.wiley.com/en-ie/System+Simulation+Techniques+with+MATLAB+and+Simulink-p-9781118694374

[49] W. Suwannahong and C. Suvanjumrat, "An integrating finite element method and multi-body simulation for drive systems analysis," Engineering Journal, vol. 21, no. 1, pp. 221–234, 2017, doi: https://doi.org/10.4186/ej.2017.21.1.221.

[50] L. M. Rodríguez-Rivera and H. F. Ruiz-Bravo, "Desarrollo de plantas virtuales para el estudio de sistemas de control usando V-REP y MATLAB®," B.S. thesis, Facultad de Ingeniería, Universidad de Nariño, Pasto, Colombia, 2020. [Online]. Available: https://sired.udenar.edu.co/7796/1/Inv.%20210536.pdf

[51] E. D. Nieto Guerrero and F. A. Vaca de la Torre, "Desarrollo de un modelo matemático, cinemático y dinámico con la aplicación de software para modificar el funcionamiento de un dron para monitoreo automático," RECIMUNDO, vol. 4, Special Issue, pp. 332–343, Mar. 2020, doi: https://doi.org/10.26820/recimundo/4.(1).esp.marzo.2020.332-343.

[52] Dassault Systèmes SOLIDWORKS Corporation, *Instructor Guide to Teaching SOLIDWORKS® Software*. Concord, MA, USA: Dassault Systèmes SOLIDWORKS Corp., 2010.

[53] C. Zhang, S. Li, and Z. Zhang, "Modeling and simulation of industrial robot arms using Simscape Multibody™," Facta Universitatis, Series: Mechanical Engineering, vol. 23, no. 2, pp. 265–286, 2025, doi: https://doi.org/10.22190/FUME230215017Z.

[54] O. E. Ramos, "Generación de trayectorias cinemáticas," Fundamentos de Robótica, 2021. [Online]. Available: https://oramosp.epizy.com/teaching/211/fund-robotica/clases/5_Generacion_Trayectorias.pdf

[55] C. D. Quintero-Guerrero, E. L. Sierra-Ballén, and W. J. Sarmiento-Manrique, "Diseño de un prototipo de sistema de realidad virtual inmersivo simplificado," Ciencia e Ingeniería Neogranadina, vol. 18, no. 1, pp. 1–16, Jun. 2008, doi: https://doi.org/10.18359/rcin.1067.

[56] Mecdata, "SprutCAM X Robot." [Online]. Available: https://mecdata.com/sprutcam-x-robot

[57] E. Pérez-Agúndez, "Ingeniería inversa y reconstrucción 3D con CATIA V5®," B.S. thesis, Universidad de Valladolid, Valladolid, Spain, Jun. 2016. [Online]. Available: http://uvadoc.uva.es/handle/10324/18096

[58] J. M. Escorcia-Hernández, "Análisis, diseño, construcción y control de un robot paralelo tipo Delta de tres grados de libertad," M.S. thesis, Universidad Politécnica de Tulancingo, Tulancingo, Mexico, Oct. 2016. [Online]. Available: https://www.upt.edu.mx/Contenido/Investigacion/Contenido/TESIS/MAC/2016/MAC_T_2016_01_JEH.pdf

[59] E. Vidal-Idiarte, A. Oller, and L. Martínez-Salamero, "Modelado y simulación de un brazo robótico," Dept. d'Enginyeria Electrònica, Elèctrica i Automàtica, Universitat Rovira i Virgili, Tarragona, Spain, Jan. 1999, doi: https://doi.org/10.13140/2.1.1352.9287.

[60] J. A. Sáinz-Cantero, "Diseño y desarrollo de un gemelo digital en Unity® 3D de una planta de reacción exotérmica y simulación de su depósito," M.S. thesis, Escuela Técnica Superior de Ingeniería, Universidad de Sevilla, Sevilla, Spain, 2024. [Online]. Available: https://ereding.etsi.us.es/bibing/proyectos/abreproy/72738/fichero/TFM-2738+Sainz-Cantero+Paredes.pdf

[61] C. García Carrascal, “Modelado y simulación con MATLAB®/Simscape™ de manipulador antropomórfico ligero LiCAS A1,” B.S. thesis, Escuela Técnica Superior de Ingeniería, Universidad de Sevilla, Sevilla, Spain, 2022.

[62] M. A. Urdaneta-Lima, “Diseño y desarrollo de un robot de inspección de tuberías,” Ph.D. dissertation, Universidad Politécnica de Madrid, Madrid, Spain, 2012, doi: https://doi.org/10.20868/UPM.thesis.14776.

[63] Dassault Systèmes SOLIDWORKS Corporation, *An Introduction to Stress Analysis Applications with SOLIDWORKS Simulation: Student Guide*. Concord, MA, USA: Dassault Systèmes SOLIDWORKS Corp., 2010. [Online]. Available: https://www.solidworks.com/sw/images/content/Training/SolidWorks_Simulation_Student_Guide-ENG.pdf

[64] J. Chirinos-Colina, *Manual de prácticas SOLIDWORKS Simulation*, 2014. [Online]. Available: https://www.academia.edu/40795849/Manual_De_Practicas_Solidworks_Simulation

[65] P. A. Ortiz Valencia, J. L. Ramírez Echavarría, and L. Cardona Rendón, *Modelo matemático y control de un sistema de fluidos*. Medellín, Colombia: Instituto Tecnológico Metropolitano, 2011, doi: https://doi.org/10.22430/9789588743080.

[66] MathWorks, “Control systems: MATLAB® and Simulink® solutions,” 2025. [Online]. Available: https://la.mathworks.com/solutions/control-systems.html

[67] A. Bayona-Gómez and F. Y. Forero-Gómez, “Diseño y construcción de un prototipo de robot móvil para navegar en terrenos irregulares,” B.S. thesis, Escuela de Ingeniería Mecánica, Universidad Industrial de Santander, Bucaramanga, Colombia, 2023. [Online]. Available: https://noesis.uis.edu.co/server/api/core/bitstreams/81f6e1cc-369b-4512-8094-688f0df465f3/content

[68] M. A. Urdaneta, C. García, R. Saltarén, G. Contreras, and R. Ugarte, “Estructura robótica pretensada para robot en tuberías petroleras,” Revista Iberoamericana de Automática e Informática Industrial, vol. 9, no. 2, pp. 135–143, 2012, doi: https://doi.org/10.1016/j.riai.2012.02.001.

[69] Schneider Electric, “Principales variables de los procesos industriales.” [Online]. Available: https://cietsa.com.mx/principales-variables-de-los-procesos-industriales/

[70] Dassault Systèmes SOLIDWORKS, “Análisis de movimiento en SOLIDWORKS.” [Online]. Available: https://es.slideshare.net/Criansiya07/Anlisis-De-Movimiento-Sw

[71] DMD, "Animaciones, estudios y análisis de movimiento en SOLIDWORKS Motion," Jan. 13, 2021. [Online]. Available: https://dmd.com.mx/2021/01/13/animaciones-estudios -y-analisis -de-movimiento-en-solidworks-motion/

[72] L. E. Herrera Galindo, "Low-power hydroelectric systems (LPHS) to energize IoT devices: A review," Ingeniería Solidaria, vol. 20, no. 1, pp. 1–35, Jan. 2024, doi: https://doi.org/10.16925/2357-6014.2024.01.10.